Scattering of light by crystals: a modified Kirchhoff approximation

Karri Muinonen

A modified Kirchhoff approximation (MKA) is developed for the scattering of light by randomly oriented crystals. The reflected and transmitted near fields are calculated from ray tracing; the corresponding far fields are then obtained via the vector Kirchhoff integral. On the shadow side of the particle, an additional near field exactly cancels the incident field and causes the forward diffraction. MKA contains a particle size dependence, which is not included in ray optics treatments, and satisfactory results can be obtained for size parameters larger than ten. The scattering phase functions and degrees of linear polarization are calculated for some hexagonal and cubic water ice crystals using MKA. The Kirchhoff approximation for particles other than crystals is discussed, and attention is paid to the backscattering enhancement due to the cyclic passage of internally or multiply externally reflected electromagnetic waves.

I. Introduction

Scattering of light by randomly oriented crystals, assumed optically homogeneous and isotropic, has recently been examined by Muinonen *et al.*,[1] hereafter referred to as Paper 1. In that work, as in other former theoretical treatises on crystal scattering,[2–8] the underlying theory was mainly geometric optics. However, in the evaluation of the forward and backward scattering peaks some physical optics corrections were introduced. In the present work, an improved approach, which is based on the Kirchhoff approximation, is established and applied to the calculation of the scattering phase functions and the degrees of linear polarization for hexagonal and cubic water ice crystals of various sizes.

The new theoretical basis, the modified Kirchhoff approximation (MKA), is developed especially for randomly oriented crystals. There are no theoretical restrictions on the application of the complete Kirchhoff approximation to the random orientation case, but the complete approximation would require about as much computer time for a single orientation as the modified version requires for random orientation. In Paper 1, the forward and backward scattering peaks were examined using a single size parameter approach. MKA introduces an extended treatment for the peaks, and in fact the former approach is an effective size parameter approximation of MKA.

MKA should prove useful in the study of light scattering from planetary atmospheres, rings, and regoliths. For example, the reason for the sharp opposition spikes of some bright satellites and the composition of the atmospheres of the outer planets can now be more reliably examined.[9,10] Still, an interesting question remains: can the cyclic passage of electromagnetic waves in the regoliths, leading to a constructive interference in the backscattering direction, cause the opposition spikes or the negative polarization branches found for some solar system objects?[11,12]

First, the Kirchhoff approximation for scattering by arbitrary small particles is introduced and discussed. Next, the modified version is developed, and the simplifications to the Kirchhoff approximation are analyzed. Then the numerical procedures are presented, and finally MKA is applied to scattering by randomly oriented hexagonal and cubic ice crystals.

II. Kirchhoff Approximation

In the Kirchhoff approximation for curved undulating surfaces, the boundary conditions are satisfied locally by assuming a Fresnelian interaction between the incident, reflected, and transmitted electromagnetic fields.[13] This means that the surface fields are calculated from phase dependent geometric optics. The Kirchhoff approximation is established for arbitrary small particles in a similar manner:

The author is with University of Helsinki, Observatory & Astrophysics Laboratory, Tähtitorninmäki, SF-00130 Helsinki, Finland.

Received 22 December 1988.
0003-6935/89/153044-07$02.00/0.

(1) The reflected and transmitted electromagnetic near fields on the surface of the scatterer are evaluated from phase dependent geometric optics.

(2) On the shadow side of the scatterer, the incident field is canceled by an additional scattered near field, which causes the forward diffraction in the radiation zone.

(3) The scattered far fields are calculated from the near fields through the vector Kirchhoff integral.[14]

At the present context the scattered near fields are assumed to be already known. The surface waves or edge scattering effects are excluded in the Kirchhoff approximation. Moreover, the Kirchhoff approximation overestimates the importance of higher order internal reflections because of the pure ray tracing treatment for the internal fields. The Kirchhoff approximation is valid for particles for which the minimum curvature of the surface is much larger than the wavelength of the incident field.

Consider now an arbitrary small particle in a fixed orientation in an incident electromagnetic plane wave field that propagates along the z axis with a wave vector $\mathbf{k}_0$ and with a harmonic time dependence $\exp(-i\omega t)$,

$$\begin{aligned}\mathbf{E}_i(\mathbf{r}) &= \mathbf{E}_0 \exp(i\mathbf{k}_0 \cdot \mathbf{r}),\\ \mathbf{B}_i(\mathbf{r}) &= \frac{1}{\omega}\mathbf{k}_0 \times \mathbf{E}_i(\mathbf{r}),\\ \mathbf{k}_0 \cdot \mathbf{E}_i(\mathbf{r}) &= \mathbf{k}_0 \cdot \mathbf{B}_i(\mathbf{r}) = 0. \end{aligned} \tag{1}$$

After the scattering process, in the radiation zone the scattered electromagnetic field is an outgoing spherical wave,

$$\mathbf{E}_s(\mathbf{r}) = \frac{\exp(ikr)}{r}\mathbf{A}(\theta,\phi) \qquad kr \gg 1, \tag{2}$$

where θ,ϕ are the scattering angles. The scattering amplitude $\mathbf{A}$ is obtained from the near fields $\mathbf{E}_s(\mathbf{r}')$ and $\mathbf{B}_s(\mathbf{r}')$ through the far field vector Kirchhoff integral,

$$\mathbf{A}(\theta,\phi) = \frac{1}{4\pi i}\mathbf{k} \times \int_{\text{surface}} dS' \left\{\frac{\omega}{k^2}\mathbf{k} \times [\mathbf{n}(\mathbf{r}') \times \mathbf{B}_s(\mathbf{r}')] - \mathbf{n}(\mathbf{r}') \times \mathbf{E}_s(\mathbf{r}')\right\} \exp(-i\mathbf{k} \cdot \mathbf{r}'), \tag{3}$$

where the integration extends over the surface of the scatterer, the unit normal of which is $\mathbf{n}(\mathbf{r}')$. The wave vector $\mathbf{k}$ points in the direction of $\mathbf{r}$. In the Kirchhoff approximation, the near fields are divided into the geometric optics and the shadow components. For example,

$$\mathbf{E}_s(\mathbf{r}') = \begin{cases}\mathbf{E}_G(\mathbf{r}') & \text{illuminated side,}\\ \mathbf{E}_G(\mathbf{r}') - \mathbf{E}_i(\mathbf{r}') & \text{shadow side.}\end{cases} \tag{4}$$

Because of the linear relation between the near and far fields, the same division can be made for the scattering amplitude,

$$\mathbf{A}(\theta,\phi) = \mathbf{A}_G(\theta,\phi) + \mathbf{A}_D(\theta,\phi),$$

$$\begin{aligned}\mathbf{A}_G(\theta,\phi) &= \frac{1}{4\pi i}\mathbf{k} \times \int_{\text{surface}} dS' \left\{\frac{\omega}{k^2}\mathbf{k} \times [\mathbf{n}(\mathbf{r}') \times \mathbf{B}_G(\mathbf{r}')] - \mathbf{n}(\mathbf{r}') \times \mathbf{E}_G(\mathbf{r}')\right\} \exp(-i\mathbf{k} \cdot \mathbf{r}'),\\ \mathbf{A}_D(\theta,\phi) &= \frac{-1}{4\pi i}\mathbf{k} \times \int_{\text{shadow}} dS' \left\{\frac{\omega}{k^2}\mathbf{k} \times [\mathbf{n}(\mathbf{r}') \times \mathbf{B}_i(\mathbf{r}')] - \mathbf{n}(\mathbf{r}') \times \mathbf{E}_i(\mathbf{r}')\right\} \exp(-i\mathbf{k} \cdot \mathbf{r}'),\end{aligned} \tag{5}$$

where $\mathbf{A}_G$ and $\mathbf{A}_D$ are the scattering amplitudes due to the geometric optics and diffraction contributions, respectively.

When the scattering amplitudes for the incident field polarized both parallel and perpendicular to the scattering plane are known, the scattering phase matrix $\bar{P}$, which relates the Stokes vectors of the incident and scattered field, and further the degree of linear polarization P and the asymmetry factor g, can immediately be calculated[1]:

$$\begin{aligned}\bar{I}_s &= \frac{\sigma_s}{4\pi r^2}\bar{P} \cdot \bar{I}_i,\\ \int_{4\pi} \frac{d\Omega}{4\pi} P_{11} &= 1,\\ P &= \frac{-P_{21}}{P_{11}},\\ g &= \int_{4\pi} \frac{d\Omega}{4\pi} \cos\theta P_{11},\end{aligned} \tag{6}$$

where σ_s is the average scattering cross section. Using the orientation angles defined in Paper 1, the integration over the orientations can be written as

$$\bar{P}(\theta) = \int_{4\pi} \frac{\sin\tau d\tau d\lambda}{4\pi} \int_{2\pi} \frac{d\phi}{2\pi} \frac{\sigma_s(\tau,\lambda)}{\sigma_s} \bar{P}(\theta,\phi;\tau,\lambda), \tag{7}$$

where $\sigma_s(\tau,\lambda)$ is the scattering cross section in the fixed orientation τ,λ. For example, the scattering phase function can be obtained from

$$P_{11}(\theta) = \int_{4\pi} \frac{\sin\tau d\tau d\lambda}{4\pi} \int_{2\pi} \frac{d\phi}{2\pi} \frac{4\pi}{\sigma_s|\mathbf{E}_0|^2} \times \tfrac{1}{2}[|\mathbf{A}_\parallel(\theta,\phi;\tau,\lambda)|^2 + |\mathbf{A}_\perp(\theta,\phi;\tau,\lambda)|^2]. \tag{8}$$

For crystal scatterers, we can proceed further by treating all the single emerging plane wavefronts separately. In a fixed orientation, the integration over the surface can thereby be divided into a number of integrations over discrete areas on the crystal faces. By marking the areas and wavefronts with the index j and including the phase information in the scattering amplitudes, we obtain

$$\mathbf{A}_G(\theta,\phi) = \sum_j \mathbf{A}_G^j(\theta,\phi)$$

$$= \sum_j \frac{1}{4\pi i}\mathbf{k}\times\int_{S_j} dS'\left\{\frac{\omega}{k^2}\mathbf{k}\times[\mathbf{n}_j(\mathbf{r}')\times\mathbf{B}_G^j(\mathbf{r}')]\right.$$

$$\left. - \mathbf{n}_j(\mathbf{r}')\times\mathbf{E}_G^j(\mathbf{r}')\right\}\exp(-i\mathbf{k}\cdot\mathbf{r}') \qquad (9)$$

$$= \sum_j \frac{1}{4\pi i}\mathbf{k}\times\left[\frac{\omega}{k^2}\mathbf{k}\times(\mathbf{n}_j\times\mathbf{B}_G^j) - \mathbf{n}_j\times\mathbf{E}_G^j\right]u_j(\mathbf{k}_j,\mathbf{k})$$

$$u_j(\mathbf{k}_j,\mathbf{k}) = \int_{S_j} dS'\exp[i(\mathbf{k}_j-\mathbf{k})\cdot\mathbf{r}'],$$

where u_j is termed the scattering integral and is closely related to the Fraunhofer diffraction integral.[15] It is straightforward to calculate the integral, when the shape and size of the surface area are known. The diffraction amplitude reads

$$\mathbf{A}_D(\theta,\phi) = \sum_j \mathbf{A}_D^j(\theta,\phi)$$

$$= \sum_j \frac{-1}{4\pi i}\mathbf{k}\times\int_{S_j} dS'\left\{\frac{\omega}{k^2}\mathbf{k}\times[\mathbf{n}_j(\mathbf{r}')\times\mathbf{B}_i(\mathbf{r}')]\right.$$

$$\left. - \mathbf{n}_j(\mathbf{r}')\times\mathbf{E}_i(\mathbf{r}')\right\}\exp(-i\mathbf{k}\cdot\mathbf{r}')$$

$$= \sum_j \frac{-1}{4\pi i}\mathbf{k}\times\left\{\frac{1}{k^2}\mathbf{k}\times[\mathbf{n}_j\times(\mathbf{k}_0\times\mathbf{E}_0)]\right.$$

$$\left. - \mathbf{n}_j\times\mathbf{E}_0\right\}u_j(\mathbf{k}_i,\mathbf{k}), \qquad (10)$$

where the summation goes over the faces that are on the shadow side of the crystal.

For particles with curved irregular surfaces, the Kirchhoff approximation leads to integration difficulties. However, an approximate stochastic treatment, resembling the one by Peltoniemi *et al.*[16] for rough particles in ray optics approximation, might be worth looking for.

The Kirchhoff approximation predicts an enhancement of backscattering due to a constructive interference for particles that are able to scatter backward through internal or multiple external reflections. This is enlightened in Fig. 1, where the waves, traveling cyclically along the path in the opposite directions, interfere constructively at the backward direction. Basically the same phenomenon has been demonstrated both experimentally and theoretically for a slab of spherical particles, where the cyclic multiple scattering between different particles causes a sharp backscattering peak.[17,18] For a single particle, the experimental verification should be straightforward, although it could include an exhaustive integration over particle orientations. Also, the phenomenon can theoretically be true for particles that do not lie in the validity region of the Kirchhoff approximation. It may also have an observable influence on the polarization in the backward scattering domain.[12]

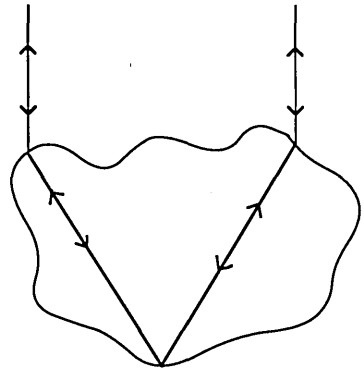

Fig. 1. Cyclic backscattering through an internal reflection.

III. Modified Kirchhoff Approximation

Instead of the complete Kirchhoff approximation, a modified approximation, which includes the most important details of the complete one and leads to numerical results, may now be introduced. The additional simplifications are briefly the following:

(1) In a fixed crystal orientation, the reflected and transmitted amplitudes are superimposed on each other, and further on the diffracted amplitude, without regard to phase.

(2) The scattering integrals are azimuthally averaged. The waves are allowed to emerge from a circular area equal to the corresponding crystal face instead of the smaller and sharp-edged real area.

(3) The diffracted amplitude is calculated from Fraunhofer's theory by assuming a size distribution of circular projected areas that is equal to the distribution of the real projected areas.

The first simplification allows us to separate the scattering phase matrix into the diffraction and the reflection and transmission parts,

$$\bar{\bar{P}} = \frac{1}{2\sigma_s}[\sigma_e\bar{\bar{P}}^D + (2\sigma_s - \sigma_e)\bar{\bar{P}}^G], \qquad (11)$$

where σ_e is the extinction cross section. In MKA it is twice the mean projected area or a half of the total surface area[19] of the randomly oriented crystal. For random crystal orientation, the constructive and destructive interferences will cancel each other quite well in directions other than the backward. MKA lacks the backscattering enhancement due to cyclic passage.

To gain insight into the significance of the second simplification, consider a plane wavefront reflected from a square face S_1 of a cubic crystal according to the geometry shown in Fig. 2. Let

$$\mathbf{E}_1(\mathbf{r}') = \mathbf{E}_1\exp(i\mathbf{k}_1\cdot\mathbf{r}'),$$

$$\mathbf{B}_1(\mathbf{r}') = \frac{1}{\omega}\mathbf{k}_1\times\mathbf{E}_1(\mathbf{r}'),$$

$$\mathbf{k}_1\cdot\mathbf{E}_1(\mathbf{r}') = \mathbf{k}_1\cdot\mathbf{B}_1(\mathbf{r}') = 0 \qquad (12)$$

be the emerging electromagnetic field on S_1. The

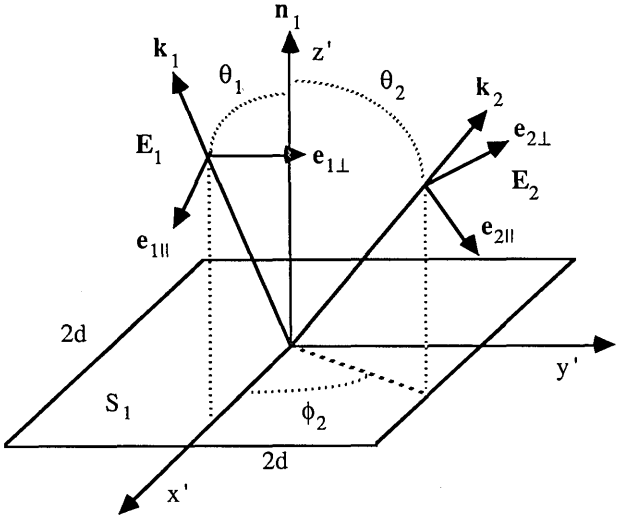

Fig. 2. Local scattering geometry on the surface element S_1.

scattering amplitude is obtained by straightforward integration,

$$\mathbf{A}_2(\theta,\phi;\tau,\lambda) = \frac{1}{4\pi i}\mathbf{k}_2 \times \left\{\frac{1}{k^2}\mathbf{k}_2 \times [\mathbf{e}_{z'} \times (\mathbf{k}_1 \times \mathbf{E}_1)] - \mathbf{e}_{z'} \times \mathbf{E}_1\right\} u_1(\mathbf{k}_1,\mathbf{k}_2), \tag{13}$$

where the scattering integral u_1 is

$$\begin{aligned} u_1(\mathbf{k}_1,\mathbf{k}_2) &= \int_{S_1} dS' \exp[i(\mathbf{k}_1 - \mathbf{k}_2)\cdot\mathbf{r}'] \\ &= 4d^2 \frac{\sin(k_{\perp x}d)}{k_{\perp x}d}\frac{\sin(k_{\perp y}d)}{k_{\perp y}d}, \\ k_{\perp x} &= k(\sin\theta_1 - \sin\theta_2\cos\phi_2), \\ k_{\perp y} &= -k\sin\theta_2\sin\phi_2. \end{aligned} \tag{14}$$

After some straightforward algebra and excluding the directions, where the far fields vanish, the following scattering matrix representation can be obtained for the relation between the reflected near and far fields predicted by the Kirchhoff approximation,

$$\begin{bmatrix} I_2 \\ Q_2 \\ U_2 \\ V_2 \end{bmatrix} = \frac{k^2}{16\pi^2 r^2}|u_1(\mathbf{k}_1,\mathbf{k}_2)|^2[(\cos\theta_1 + \cos\theta_2)^2 + \sin^2\theta_1 \sin^2\theta_2 \sin^2\phi_2] \times \begin{bmatrix} 1 & 0 & 0 & 0 \\ 0 & \cos 2\eta & \sin 2\eta & 0 \\ 0 & -\sin 2\eta & \cos 2\eta & 0 \\ 0 & 0 & 0 & 1 \end{bmatrix}\begin{bmatrix} I_1 \\ Q_1 \\ U_1 \\ V_1 \end{bmatrix}, \tag{15}$$

$$\cos\eta = \frac{\cos\phi_2(\cos\theta_1 + \cos\theta_2)}{\sqrt{(\cos\theta_1 + \cos\theta_2)^2 + \sin^2\theta_1 \sin^2\theta_2 \sin^2\phi_2}},$$

$$\sin\eta = \frac{\sin\phi_2(1 + \cos\theta_1\cos\theta_2)}{\sqrt{(\cos\theta_1 + \cos\theta_2)^2 + \sin^2\theta_1 \sin^2\theta_2 \sin^2\phi_2}}.$$

It is evident from both Eqs. (13) and (15) that the size dependence is included only in the scattering integral, which thereby determines the spreading of the reflected plane wavefront. In MKA, an approximation is developed both for the squared scattering integral and the angular term in front of the rotation matrix in Eq. (15). Thus, instead of the square area S_1, consider next a circular area S_R of equal size with radius R in an otherwise equivalent situation; in that case the scattering integral leads to

$$\begin{aligned} u_R(\mathbf{k}_1,\mathbf{k}_2) &= \int_{S_R} dS' \exp[i(\mathbf{k}_1 - \mathbf{k}_2)\cdot\mathbf{r}'] = \pi R^2 \frac{2J_1(k_\perp R)}{k_\perp R}, \\ k_\perp &= k\sqrt{\sin^2\theta_1 + \sin^2\theta_2 - 2\sin\theta_1\sin\theta_2\cos\phi_2}, \\ R &= \frac{2d}{\sqrt{\pi}}. \end{aligned} \tag{16}$$

For external reflection from the square crystal face, the second simplification to the Kirchhoff approximation can now be written as

$$\begin{aligned} |u_1(\mathbf{k}_1,\mathbf{k}_2)|^2[(\cos\theta_1 + \cos\theta_2)^2 + \sin^2\theta_1\sin^2\theta_2\sin^2\phi_2] \approx \\ |u_R(\mathbf{k}_1,\mathbf{k}_2)|^2[(\cos\theta_1 + \cos\theta_2)^2 + \sin^2\theta_1\sin^2\theta_2\sin^2\phi_2] \approx \\ \frac{4\pi^2R^2}{k^2}\cos\theta_1 p_{11}(\mathbf{k}_1,\mathbf{k}_2), \end{aligned} \tag{17}$$

where p_{11}, the scattering function, reads

$$\begin{aligned} p_{11}(\mathbf{k}_1,\mathbf{k}_2) &= x_1^2\cos(\mathbf{k}_1,\mathbf{k}_2)\left\{\frac{2J_1[x_1\sin(\mathbf{k}_1,\mathbf{k}_2)]}{x_1\sin(\mathbf{k}_1,\mathbf{k}_2)}\right\}^2 \Theta[90° - (\mathbf{k}_1,\mathbf{k}_2)] \\ &\quad + J_0(x_1)^2 + J_1(x_1)^2, \\ x_1 &= kR\sqrt{\cos\theta_1} \end{aligned} \tag{18}$$

and has the following asymptotic and normalization properties:

$$\begin{aligned} p_{11}(\mathbf{k}_1,\mathbf{k}_2) &= 4\pi\delta(0°) \quad x_1 \gg 1, \\ p_{11}(\mathbf{k}_1,\mathbf{k}_2) &= 1 \qquad\quad x_1 \ll 1, \\ \int_{4\pi}\frac{d\Omega}{4\pi}p_{11} &= 1. \end{aligned} \tag{19}$$

In MKA the scattering matrix representation for the reflected near and far fields reads thereby

$$\begin{bmatrix} I_2 \\ Q_2 \\ U_2 \\ V_2 \end{bmatrix} = \frac{\pi R^2}{4\pi r^2}\cos\theta_1 p_{11}(\mathbf{k}_1,\mathbf{k}_2)\begin{bmatrix} 1 & 0 & 0 & 0 \\ 0 & \cos 2\eta & \sin 2\eta & 0 \\ 0 & -\sin 2\eta & \cos 2\eta & 0 \\ 0 & 0 & 0 & 1 \end{bmatrix}\begin{bmatrix} I_1 \\ Q_1 \\ U_1 \\ V_1 \end{bmatrix}, \tag{20}$$

where the η angle is defined in Eq. (15).

The approximate scattering function is compared to the exact one, which is distinguishable from Eq. (17),

in Fig. 3 in the x'–z' plane for a size parameter $kR = 10$ and for three angles of emergence, $\theta_1 = 0$, 30, and 60°. The differences rise mainly from the rotational symmetry of the approximate pattern around the initial propagation direction. In the exact pattern the peak maximum appears at a smaller angle of emergence than the initial, which is not included in MKA, and can cause some error in the calculations. For the oblique emergence, the smaller projected area is taken into account and leads to further spreading of the wavefronts, as seen in the figure.

The calculation of the projected areas for the transmitted plane wavefronts has been excluded, which is by far the largest simplification in MKA. Instead, the spreading is described with the scattering function stated in Eq. (18) separately for each crystal face. This means that the spreading of the transmitted waves is underestimated, since their real projected areas must be smaller than the crystal face areas in question. However, the choice for the scattering function ensures that MKA approaches ray optics with increasing size parameter. The low size parameter limit is sensitive to the approximations made in formulating the scattering function. Here an isotropic asymptotic limit has been adapted. The circular approximation fails for elongated surface areas, which restricts the applicability of MKA.

Finally, the diffraction part of the scattered intensity is approximated as

$$P_{11}^{D}(\theta) \approx \int dyn(y)\,\frac{\pi y^2}{\pi x^2}\left\{y^2\cos\theta\left[\frac{2J_1(y\sin\theta)}{y\sin\theta}\right]^2\Theta(90^\circ-\theta) + J_0(y)^2 + J_1(y)^2\right\},$$

$$\int dyn(y) = 1, \tag{21}$$

where n is the normalized size parameter distribution for projected areas of the randomly oriented crystal, and x is the mean projected area size parameter. Takano and Asano[20] have compared the Fraunhofer diffraction by hexagonal scatterers to the diffraction by spheres. In the present context, the precision of the equal sphere approximation is satisfactory, and this choice for the diffraction calculation is consistent with the treatment of the reflected and transmitted waves.

IV. Numerical Analysis

The geometric optics ray tracing in the present calculations is similar to that presented in Paper 1 up to the stage where the ray leaves the crystal. There, a Monte Carlo technique has been introduced for the scattering process stated in Eq. (20). For a unit initial irradiance, a cutoff value of 10^{-4} and a ray index maximum of one hundred have been used, which has allowed a computational loss of <0.1% of the initial energy. The number of rays traced in each case has been around 5×10^6, which has taken ~5 h of CPU time on a VAX 8800. The estimated relative accuracy for the computations has been better than 2%. A 1° angular resolution has been found to be satisfactory for the particle sizes included elsewhere than in the exact forward and backward directions, where a resolution of 0.05° has been used. The size parameter distribution for the diffraction calculation has been computed during the ray tracing. If necessary, a more effecient treatment can be achieved by computing the scattering by crystals of different sizes simultaneously during a single ray tracing procedure.

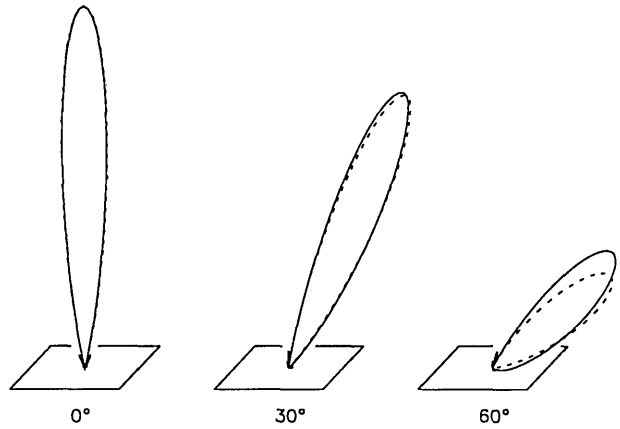

Fig. 3. Comparison between the exact (solid line) and approximate (dotted line) scattering functions for the square element S_1 in Fig. 1 in the x'–z' plane. The size parameter is $kR = 10$. Notice the gradual deterioration of the approximation with increasing angle of emergence.

V. Results

The scattering phase functions and degrees of polarization for hexagonal plates with c:$2a$ = 1:2 and cubic crystals of water ice for mean size parameters of 25, 100, and 400 are presented in Figs. 4 and 5, respectively. The asymmetry factors, the phase function values at 0 and 180°, and the polarization minimums and maximums are summarized in Table I. Similarities to the results obtained by Hansen and Travis for spheres[21] and Takano and Tanaka for circular cylinders[22] are obvious.

Due to the corner retroreflection capability of the cubic crystals, their asymmetry factors are smaller than those of the hexagonal ones. A slight increase of the asymmetry factor with increasing size parameter is also observed for both crystal types. This arises partially from sharpening of the diffraction with increasing size parameter.

For the plate, the major size parameter dependence of the phase function is concentrated on the peak and halo regions. For the smallest size parameter, it is evident that neither the 22 or 46° halos are distinguishable from the diffraction ripple structure. The backscattering peak is spread over a wide interval, and one can hardly speak about any peak at all. For the medium size parameter, the geometric optics effects are already clear. The halos and backscattering peak show up in the pattern, although some diffraction ripple structure disturbs the otherwise smooth curve. For the largest size parameter, the calculations lead to a pattern that closely resembles ray optics results.

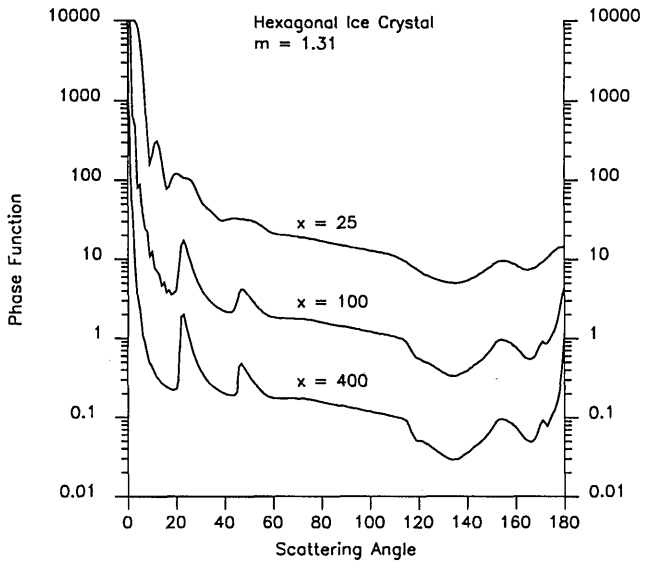

(a)

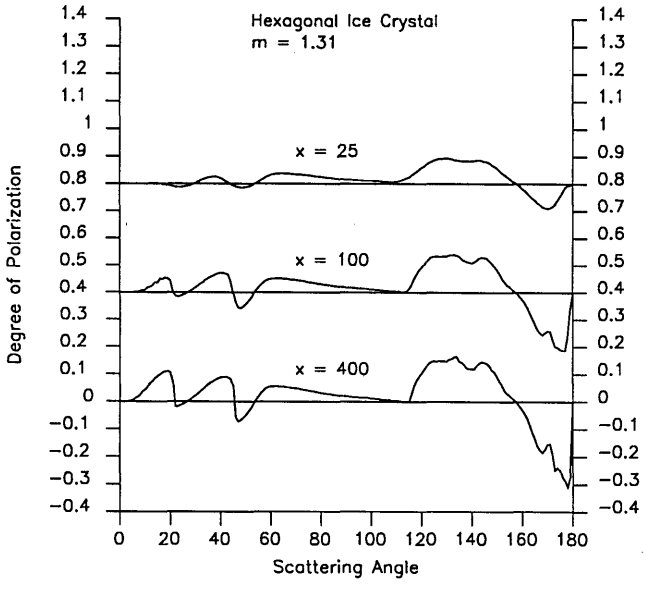

(b)

Fig. 4. Scattering phase function (a) and degree of polarization (b) for hexagonal ice plates. The halos and peaks in the phase function sharpen, and the amplitude of the polarization increases with increasing size parameter. For better display of the results, the phase functions have been multiplied by factors of 50.0, 5.0, and 0.5, and the constants 0.8, 0.4, and 0.0 have been added to the polarization of the order of increasing size parameter (see Table I).

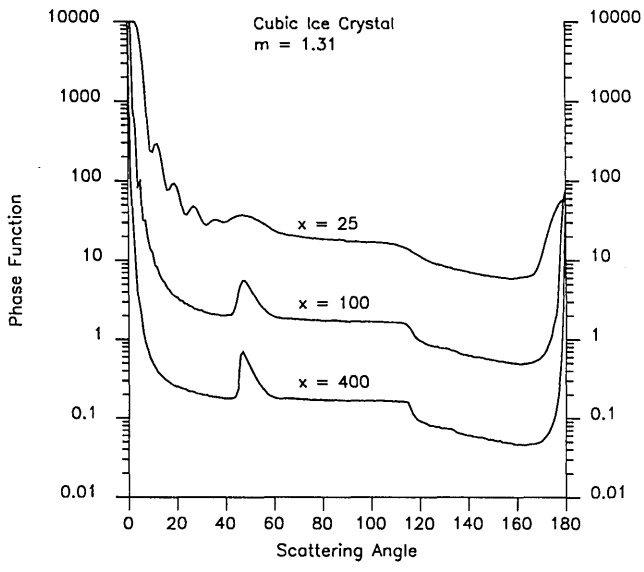

(a)

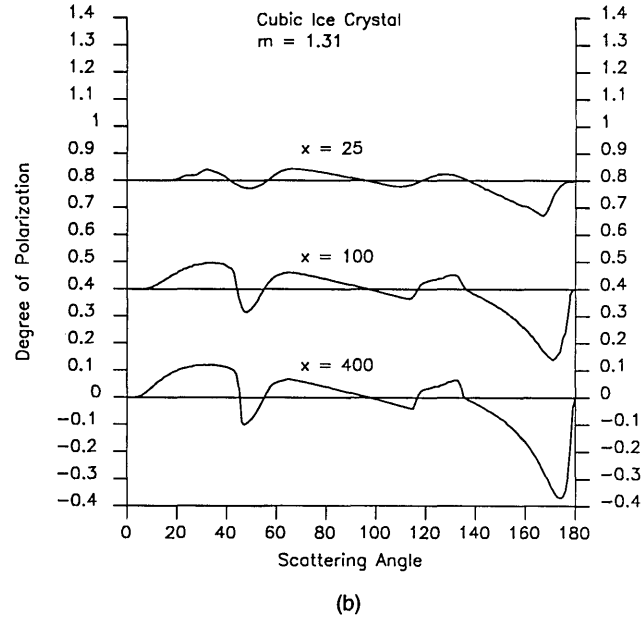

(b)

Fig. 5. Scattering phase function (a) and degree of polarization (b) for cubic ice crystals. Notice the diffraction ripple structure and backscattering peak formation. The display is the same as in Fig. 4 (see Table I).

The neutralization of the polarization with decreasing size parameter can be readily recognized. The neutral polarization is in qualitative agreement with the experiments by Perry *et al.*[23] for NaCl particles. MKA predicts that the derivatives of the polarization patterns at the forward and backward directions are continuous, which means that the first derivatives must vanish. Because of the wide angular display interval, this can be seen only for the lowest size pa-

Table I. Asymmetry Factors g, the Phase Function Values at 0 and 180°, and the Polarization Minimums P_{min} and Maximums P_{max} for Ice Cubes and Plates with Given Size Parameter x

	Ice cubes			Ice plates		
	$x = 25$	$x = 100$	$x = 400$	$x = 25$	$x = 100$	$x = 400$
g	0.72	0.73	0.74	0.78	0.79	0.79
$P_{11}(0°)$	3.7×10^{2}	6.0×10^{3}	9.5×10^{4}	4.0×10^{2}	6.3×10^{3}	1.0×10^{5}
$P_{11}(180°)$	1.2×10^{0}	1.6×10^{1}	2.5×10^{2}	2.9×10^{-1}	8.6×10^{-1}	3.5×10^{0}
P_{min}	−0.13	−0.26	−0.37	−0.09	−0.21	−0.31
P_{max}	0.04	0.10	0.12	0.09	0.14	0.16

rameter. The negative polarization branch in the backward domain grows wider with the increasing size parameter.

For the cube, effects similar to those for the hexagonal plate show up in the patterns. However, the trough retroreflection forms only some background contribution in the phase function because of the predominance of the corner retroreflection. On the other hand, the former affects the polarization considerably, and the influence increases with increasing size parameter.

The smoothing of the curves due to the finite size of the scatterers is the most important improvement to ray optics. Still, ray optics predicts the overall behavior of the phase function and the polarization, excluding the halo and peak regions, surprisingly well, which is mostly due to the locally planar character of the crystal surface.

VI. Conclusions

A modified Kirchhoff approximation, or MKA, has been developed for the scattering of light by randomly oriented crystals. MKA includes a particle size dependence superior to ray optics, as has been demonstrated via the calculation of the scattering phase function and the degree of linear polarization for hexagonal and cubic ice crystals. The main results were a slight decrease of the asymmetry factor, a spreading of the peaks and halos in the phase function, and the neutralization of polarization, all with decreasing mean size parameter.

MKA has been developed especially for randomly oriented crystals. The method approaches ray optics with increasing size parameter, while for small size parameters isotropic scattering is predicted. However, MKA is applicable only to large crystals, i.e., crystals with the mean size parameter larger than ten, and experimental verification of the validity of MKA is clearly needed. At the moment, the treatment for light scattering by crystals in the complete Kirchhoff approximation requires too much computer time, but it may be possible in the future.

I thank Kari Lumme, Jouni Peltoniemi, and William M. Irvine for valuable suggestions. This work was supported by NASA grant NGL 22-010-023.

References

1. K. Muinonen, K. Lumme, J. Peltoniemi, and W. M. Irvine, "Light Scattering by Randomly Oriented Crystals," Appl. Opt. **28,** 3051–3060 (1989).
2. H. Jacobowitz, "A Method for Computing the Transfer of Solar Radiation through Clouds of Hexagonal Ice Crystals," J. Quant. Spectrosc. Radiat. Transfer **11,** 691–695 (1971).
3. P. Wendling, R. Wendling, and H. K. Weickmann, "Scattering of Solar Radiation by Hexagonal Ice Crystals," Appl. Opt. **18,** 2663–2671 (1979).
4. K. N. Liou, *An Introduction to Atmospheric Radiation* (Academic, New York, 1980).
5. Q. Cai and K.-N. Liou, "Polarized Light Scattering by Hexagonal Ice Crystals: Theory," Appl. Opt. **21,** 3569–3580 (1982).
6. K. N. Liou, Q. Cai, P. W. Barber, and S. C. Hill, "Scattering Phase Matrix Comparison for Randomly Hexagonal Cylinders and Spheroids," Appl. Opt. **22,** 1684–1687 (1983).
7. K. N. Liou, Q. Cai, J. B. Pollack, and J. N. Cuzzi, "Light Scattering by Randomly Oriented Cubes and Parallelepipeds," Appl. Opt. **22,** 3001–3008 (1983).
8. Y. Takano and K. Jayaweera, "Scattering Phase Matrix for Hexagonal Ice Crystals Computed from Ray Optics," Appl. Opt. **24,** 3254–3263 (1985).
9. K. Lumme, K. Muinonen, J. Peltoniemi, H. Karttunen, and E. Bowell, "A Possible Explanation for the Anomalously Sharp Opposition Effects," BAAS 19, 850–850 (1987).
10. K. Muinonen, K. Lumme, and J. Peltoniemi, "Scattering of Light by Crystals: A Possible Application to Planetary Dust," accepted for Adv. Space Res. (1988).
11. B. Lyot, "Recherches sur la Polarisation de la Lumiére des Planétes et de Quelques Substances Terrestres," Ann. Obs. Paris 8(1), (1929).
12. K. Muinonen, "Electromagnetic Scattering by Two Interacting Dipoles," accepted to the Proceedings of the 1989 URSI EM Theory Symposium (1989).
13. A. Ishimaru, *Wave Propagation and Scattering in Random Media* (Academic, New York, 1978).
14. J. D. Jackson, *Classical Electrodynamics* (Wiley, New York, 1975).
15. M. Born and E. Wolf, *Principles of Optics* (Pergamon, New York, 1959).
16. J. I. Peltoniemi, K. Lumme, K. Muinonen, and W. M. Irvine, "Scattering of Light by Stochastically Rough Particles," accepted for Appl. Opt. (1989).
17. Y. Kuga and A. Ishimaru, "Retroreflectance from a Dense Distribution of Spherical Particles," J. Opt. Soc. Am. A **1,** 831–835 (1984).
18. L. Tsang, J. A. Kong, and R. T. Shin, *Theory of Microwave Remote Sensing* (Wiley, New York, 1985).
19. H. C. van de Hulst, *Light Scattering by Small Particles* (Wiley, New York, 1957).
20. Y. Takano and S. Asano, "Fraunhofer Diffraction by Ice Crystals Suspended in the Atmosphere," J. Meteorol. Soc. Jpn. **61,** 289–300 (1983).
21. J. E. Hansen and L. D. Travis, "Light Scattering in Planetary Atmospheres," Space Sci. Rev. **16,** 527–610 (1974).
22. Y. Takano and M. Tanaka, "Phase Matrix and Cross Sections for Single Scattering by Circular Cylinders: a Comparison of Ray Optics and Wave Theory," Appl. Opt. **19,** 2781–2793 (1980).
23. R. J. Perry, A. J. Hunt, and D. R. Huffman, "Experimental Determinations of Mueller Scattering Matrices for Nonspherical Particles," Appl. Opt. **17,** 2700–2710 (1978).